Modelling sensory integration for ankle- and hip control in human balance

Peterke van der Zwaag

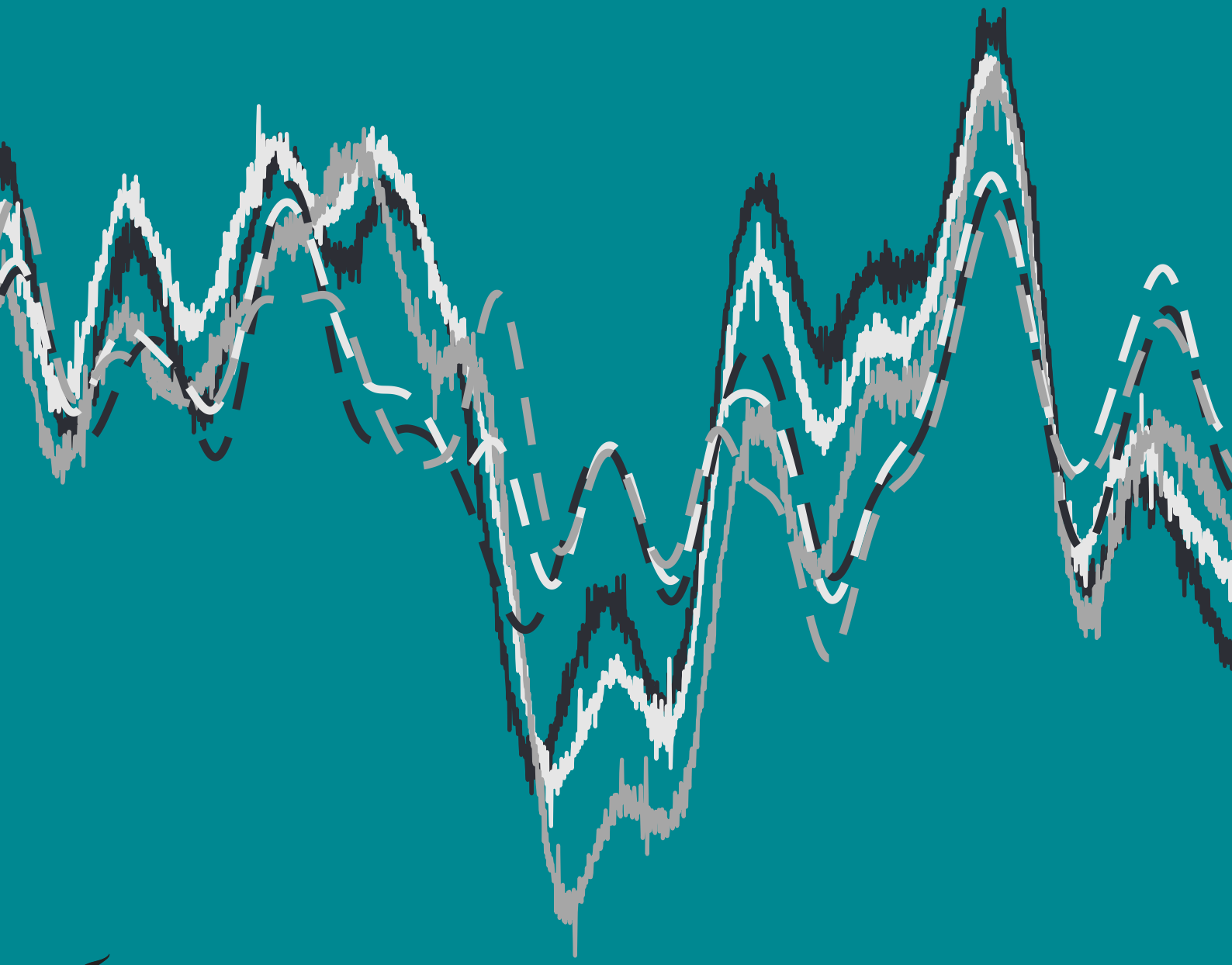

TU Delft

Modelling sensory integration for ankle- and hip control in human balance

by

Peterke van der Zwaag

to obtain the degree of Master of Science
at the Delft University of Technology,
to be defended publicly on Wednesday April 17, 2019 at 15:00.

Student number: 4159675

Thesis committee:

Prof. dr. ir. A. C. Schouten,	TU Delft, supervisor
J. van Kordelaar PhD,	TU Delft, supervisor
Dr. D. Dodou,	TU Delft, External Committee Member
Dr. ir. M. M. van Paassen,	TU Delft, External Committee Member

TU Delft

Preface

Before presenting my thesis, I would like to take the opportunity to thank some people who helped me during my thesis project.

First of all, I would like to thank my supervisors, Alfred Schouten, Joost van Kordelaar and Jantsje Pasma, for their guidance throughout the project. I appreciate all the productive conversations and all the helpful tips and feedback. Furthermore, all three of you always made time to read parts of my paper or to meet with me on short notice when I was stuck or needed extra help, and I valued that a lot.

I would like to thank "The Squad" for being my study buddies throughout the last year. Without the social obligation to be present every morning, the lunch- and coffee breaks in which we (almost) never talked about thesis-related stuff and the occasional parties, this project would have probably taken me a lot longer. I would like to give a special thanks to Simon van der Helm, who helped me stick to my planning and provided a lot of valuable input throughout every stage of the project.

Lastly, I would like to thank my family for always and unconditionally supporting me throughout the 7.5 years of my studies.

Peterke van der Zwaag
Delft, April 2019

Modelling sensory integration for ankle- and hip control in human balance

Peterke van der Zwaag

***Abstract*—Falling is a problem in elderly, affecting 30% of people over 65 years old, and leading to serious injuries in 10% of the cases. Because balance is controlled in a closed loop system with a high level of redundancy, the cause of impaired balance control is often unknown. A balance control model in combination with perturbed balance experiments could be a useful aid to detect the underlying cause of balance impairment, which would allow for better treatment. A disturbance estimation and compensation (DEC) model has a strong neurological basis and is able to describe multiple conditions with one set of parameters.**

An existing DEC model, containing separate ankle and hip control, was extended by adding visual and mechanical disturbance estimations. The model was fitted to experimental data of elderly subjects maintaining balance in three conditions containing four disturbances simultaneously; visual and ankle proprioceptive perturbations and mechanical perturbations at the hip and shoulder level. To validate the fitting procedure, the model parameters were also fitted to data simulated by the model, and a sensitivity analysis was done.

Being fitted to experimental data, the model could reproduce about 60% of the behaviour. Mainly the low frequency behaviour could not fully be tracked. Parameter estimation proved challenging, with some parameters consistently estimated larger or smaller than expected or physiologically plausible. Fitting the model on its own simulated data could reproduce $>$99.9% of the behaviour, but with some parameters consistently estimated up to a factor 10 too small or too large.

Many adaptations and extensions to the existing DEC model were made simultaneously and with the available experimental data it was not possible to investigate the individual influence of each adaptation. If a broader range of experimental data is available, with conditions where only one, two or three perturbations are applied, it is possible to validate each model adaptation separately. This would likely improve the model. With the suggested improvements, the multisegmental DEC model opens up the way towards better treatment for balance impairment.

I. Introduction

Falling is a serious problem in elderly [1]. Of people aged over 65 years old, about 30% fall at least once a year [2], [3], [4], leading to serious injuries in about 10% of the cases [5] or even death [6]. Serious injuries include fractures and subdural haematomas. Impaired standing balance control is one of the main causes of falling [5]. Unfortunately, the cause of impaired balance control is often unknown.

Human balance in the sagittal plane is inherently unstable, because any disturbance causes the centre of mass (COM) to move from its equilibrium position and subsequently creates a moment around the ankle joint in the same direction, which leads to a fall if it is not corrected. The intrinsic stiffness of the ankle joint is not enough to keep a person stable [7], so humans need to actively control the muscles around their ankles to maintain a standing position. To efficiently control their balance, humans have a sophisticated, closed loop balance control system, of which a schematic overview is shown in Figure 1. The vestibular system is used to measure the orientation and acceleration of the head relative to the direction of gravity. Visual information is used to determine the position of the head relative to the visible environment. Proprioception is done by two types of sensors, muscle spindles and Golgi tendon organs. Muscle spindles measure the angles between the different body segments relative to each other. The measured angles are used to determine the orientation of the rest of the body from the head orientation [8]. Golgi tendon organs measure the amount of active torque produced by the muscles. Lastly, the somatosensory system can determine the amount of active ankle torque from the centre of pressure (COP) on the foot soles.

There are two reasons why identification of impairments in the balance control system is difficult. The first is inherent to closed loop systems; the source of errors is difficult to determine from the output. Disturbances can enter the balance control system via noisy or incorrect signals in different systems, and errors in different involved systems can result in the same symptoms. Thus determining the cause of symptoms cannot easily be done. For example, decreased muscle mass and increased neural time delays both cause increased body sway [9], [10]. The second difficulty is that there is a high level of redundancy present in the balance control system. Redundancy allows for compensation strategies in the presence of impairments. For example, in the presence of decreased vestibular function, there is an increased reliance on the visual information [11],

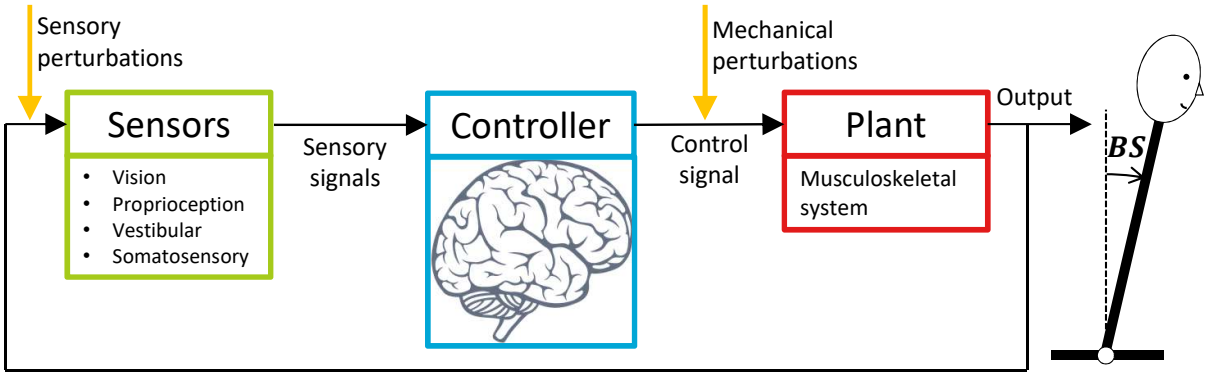

Figure 1: Schematic representation of the control system that humans use to control their balance. The control system consists of three main elements, which are linked in a closed loop feedback system. Sensory systems provide the feedback by measuring some information about the state of the system, which is the position of the body relative to its environment. The nervous system uses the information from the sensory systems to generate motor commands that direct the body toward the equilibrium position. The musculoskeletal system is the plant that generates the actual movement of the body. Sensory and mechanical perturbations can be applied.

which in turn can mask impairments that are present.

Currently, two methods exist that are used by clinicians to assess balance impairment: static and dynamic posturography. In static posturography tests, patients are asked to perform tasks such as maintaining balance with their eyes closed or on a narrow platform. These tests are inexpensive and easy to conduct because no advanced equipment is necessary. Dynamic posturography tests, such as the sensory organization test [12], are more advanced and involve patients standing in balancing devices. Dynamic conditions include body sway referencing a visual screen and/or the base plate, disabling visual or proprioceptive information or both. During experiments, body sway and pressure distribution on the foot soles are measured. Although both clinical methods are capable of describing the symptoms of balance impairment, neither can detect the underlying cause of the impairment. To improve treatment using targeted interventions, it would be useful to know what the underlying cause of impaired balance control is.

Perturbed posturography, a third type of posturography, can help open the control loop. In perturbed posturography, different reactions are measured to different, well known, perturbations in an experimental setup. Closed loop system identification techniques can be applied to the data to determine the effect of the different perturbations [13]. The Balance test Room (BalRoom), shown in Figure 2, is a sophisticated balance room that was designed to perturb and measure human balance in many different conditions [13]. Four disturbances can be applied to a subject at once: Visual screen rotation, base plate rotation, and mechanical pushes to the hips and shoulders. Simultaneously, body sway is measured at the hip and shoulder level, allowing sway of the legs and trunk to be measured separately. This extra degree of freedom adds much value to the experiments. It has been shown that balance impairment influences the intersegmental coordination [14], [15], indicating that measuring ankle and hip angles separately is necessary to identify underlying impairment.

BalRoom data has already been used for system identification purposes, by determining the frequency

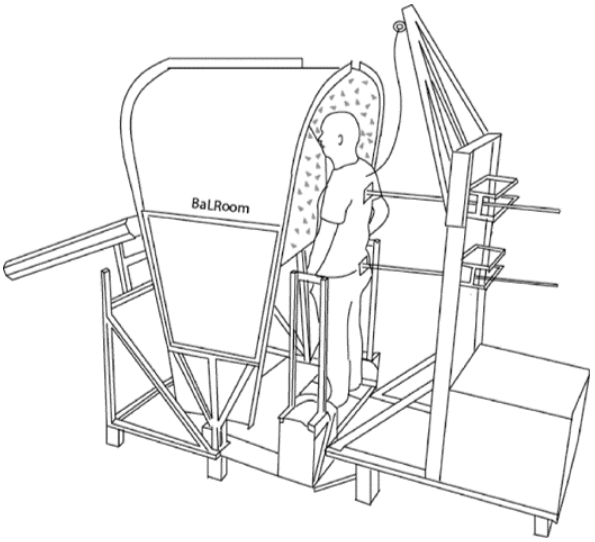

Figure 2: Schematic figure of the BalRoom. Subjects stand on a rotating base plate in front of a rotating visual screen while subjected to mechanical forces to the hips and shoulders and while wearing a safety harness. Figure was taken from [13].

response functions (FRFs) of the applied perturbations. However, no parameter estimation has been done. For clinical purposes, it is necessary to analyze the data in a way that gives physical or physiological meaning to the parameters. A balance control model is a powerful tool that can give physical and physiological meaning to the BalRoom data.

The Disturbance Estimation and Compensation (DEC) model was developed from a neurological background and was first presented in 2003 [16]. The model is nonlinear and combines sensory input signals to make estimates of disturbances that are present in or applied to the body, for example a body sway angle forward or backward, or a foot space tilt angle different from horizontal. The disturbance estimations are scaled with a gain between 0 and 1, to reflect the quality of the signal, and a detection threshold is applied to the signal, which is hypothesized to be the method in which the neural system distinguishes between noise and relevant disturbances [16].

What makes the DEC model unique, is that the model structure provides the sensory reweighting that is present in human balance. Sensory reweighting is responsible for the adaptation to sensory disturbances, such as the saturation in body sway amplitude in the presence of visual disturbances with increasing amplitude [11]. This means that only one set of parameters is necessary to describe balance in different conditions. This is in contrast to other commonly used balance control models, such as the independent channel (IC) model [17], in which different conditions are explained with different weights for the sensory channels.

The DEC model has mainly been used as a single segment model around the ankle joint [16], [18], [19]. One multisegmental DEC model has been published with both an ankle and hip joint [20]. The published model can only be applied to a limited amount of experimental conditions because it does not incorporate vision or external forces applied to the body. However, because of its modular nature, the model can be extended to make it applicable to conditions that are applied by the BalRoom.

Experimental conditions of multiple perturbations signals and multisegmental body sway measurement in multiple conditions are exactly the experimental conditions that are necessary for detecting balance impairment [13]. Therefore, if we can apply the DEC model to the BalRoom data in multiple conditions, this indicates that the DEC model is also a strong candidate for application in detecting balance impairment. However, the application of the DEC model to BalRoom data is challenging. It has never been attempted to fit a multisegmental balance control model to experimental data in conditions with so many disturbances at once. The scientific gap that this study aims to fill is captured in the following research question:

"To what extent is the DEC model able to capture human balance in the presence of visual, proprioceptive and mechanical disturbances, with different conditions of applied perturbations?"

To answer this question, data was used of elderly subjects in the BalRoom with three different perturbation conditions and the multisegmental DEC model was extended to incorporate visual and mechanical disturbances. The method section describes the adaptations of the DEC model and the procedure that was used to fit and validate the model. The results show that although some changes are necessary, the DEC model is indeed a promising tool for finding underlying cause of balance impairment.

II. Method

The goal of this study is to fit the DEC model to BalRoom data. To this end, the research method consisted of several steps. The first was the collection of experimental data recorded with the BalRoom. The second was the development of the extended multisegmental DEC model. The third step was the design of a fitting procedure, which was used for several purposes. The first was to find parameter values that produce stable simulations. Then, the model was fitted to the BalRoom data. The model was also fitted to its own simulated data and a sensitivity analysis was done.

A. Experimental data

Experimental data used for this research was available from a previous study that investigated the reliability of closed loop system identification techniques to assess balance control [13].

1) Subjects: Experiments were done with 12 participants aged 70 years or older. All participants were healthy and had no existing balance impairment. Participants were excluded in the case of low cognitive function (Mini Mental State Examination (MMSE) $\leq$ 26 [13], [21]), clinical significant morbidity, postural hypotension and use of medication. The experiment was approved by the Medical Ethics Committee of Leiden University Medical Centre and was performed in accordance with the principles of the Declaration of Helsinki and the International Conference on Harmonization/Good Clinical Practice (ICH/GCP) [13]. All subjects gave written informed consent [13].

2) Experimental setup: The BalRoom device is able to measure perturbed stance by performing several perturbations and measurements all at once. Four perturbations can simultaneously be applied to a subject. A visual screen can rotate around the ankle axis, creating

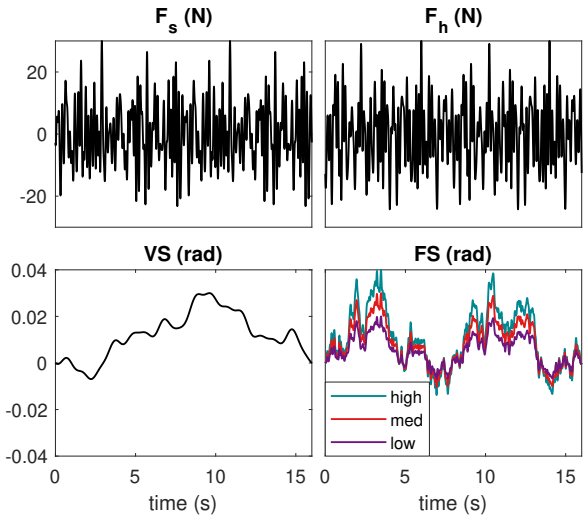

Figure 3: Perturbation signals applied to the subjects. The force perturbation applied to the shoulders (F_s), the force applied to the hips (F_h), the visual screen tilt (V) are the same for all experiments. The support surface rotation (FS) is varied between high (zero-to-peak amplitude of 0.04 rad), medium (0.03 rad) and low (0.02 rad).

a visual perception of body sway. The base plate on which the subject stands can also rotate around the ankle axis, disturbing the ankle proprioception that is used to estimate body sway [9]. The remaining two disturbances that can be applied are mechanical pushes and pulls applied by two rods, one at the hip level and one at the shoulder level. Measurements that are performed include the body sway measurement in the sagittal plane at the hip and shoulder level, thereby measuring the sway of the leg and head-arms-trunk (HAT) segment separately. Lastly, the base plate rotation and the rod forces are measured to quantify the applied disturbances.

The experimental protocol was extensive and included many experiments, but only a fraction of the data was necessary for this study. The first session on the first day was chosen to serve as the data for this study, to minimize learning effects present in the data. The session consisted of three trials with different base plate rotation (FS) amplitudes.

The leg length (l_l), trunk length (l_t), shoulder height (h_s) and body mass (m_b) were measured for all subjects. Other biomechanical parameters were estimated from the measured parameters using the body anthropometrics from [22].

3) Perturbation and response signals: All four perturbations were applied simultaneously. All perturbations were multisine signals, each containing different frequencies. The signals are shown in Figure 3. The perturbation signals have a duration of 16 seconds. Each trial, the same perturbation signals are repeated eight times, resulting in trials with a duration of 128 seconds. Sampling was done at a frequency of 1000 Hz. Every trial, the perturbation signals start at some point within the 16-second time frame of the signals. The starting point of the perturbation signals is random, but is always the same for all for four perturbation signals within one trial. Therefore, the starting point is different for each trial, but the mutual timing of the four perturbation signals is always the same. A window of seven perturbation cycles was selected from each trial so that all experiments start at time point 0 within the perturbation signals in Figure 3, where all signals have a value of 0. The average of the measured perturbations, FS, F_s, and F_h, was taken from the experimental data as the input of the simulations. Because VS is not measured, the theoretical signal was used.

The average over the seven perturbation repetitions was also taken of the two responses, the trunk segment angle (TS) and the leg segment angle (LS) relative to space. These signals serve as the signals for the model to fit on. Body sway was measured with string potentiometers, of which the exact length of the string is unknown. Therefore, it was not possible to reconstruct the absolute angles. To eliminate the effect of a possible offset, both the experimental body sway signals and the simulated body sway signals were made zero-mean signals.

B. Model

The principle of a DEC model is that the model structure provides the sensory reweighting that is observed in human balance control. Only one multi-segmental DEC model has been published yet [20], which was used as the basis for the model developed in this study. The model was extended to describe human balance in a wider variety of conditions and several improvements were made. The model was implemented in Matlab Simulink (The MathWorks, Natick, MA, United States) and is shown in Figure 4. A large number of parameters determine the behaviour of the model. An extensive description of the model is given in Appendix A. The short description of the model, focused on the elements that are different from the published model [20], is given below. A list of parameters and their abbreviations can be found in Tables AI, AII, AIII and AIV in Appendix A.

1) Model description: As shown in Figure 4, physical variables, represented in capital letters, enter the control system through the sensory systems. The internal representations of the physical variables are

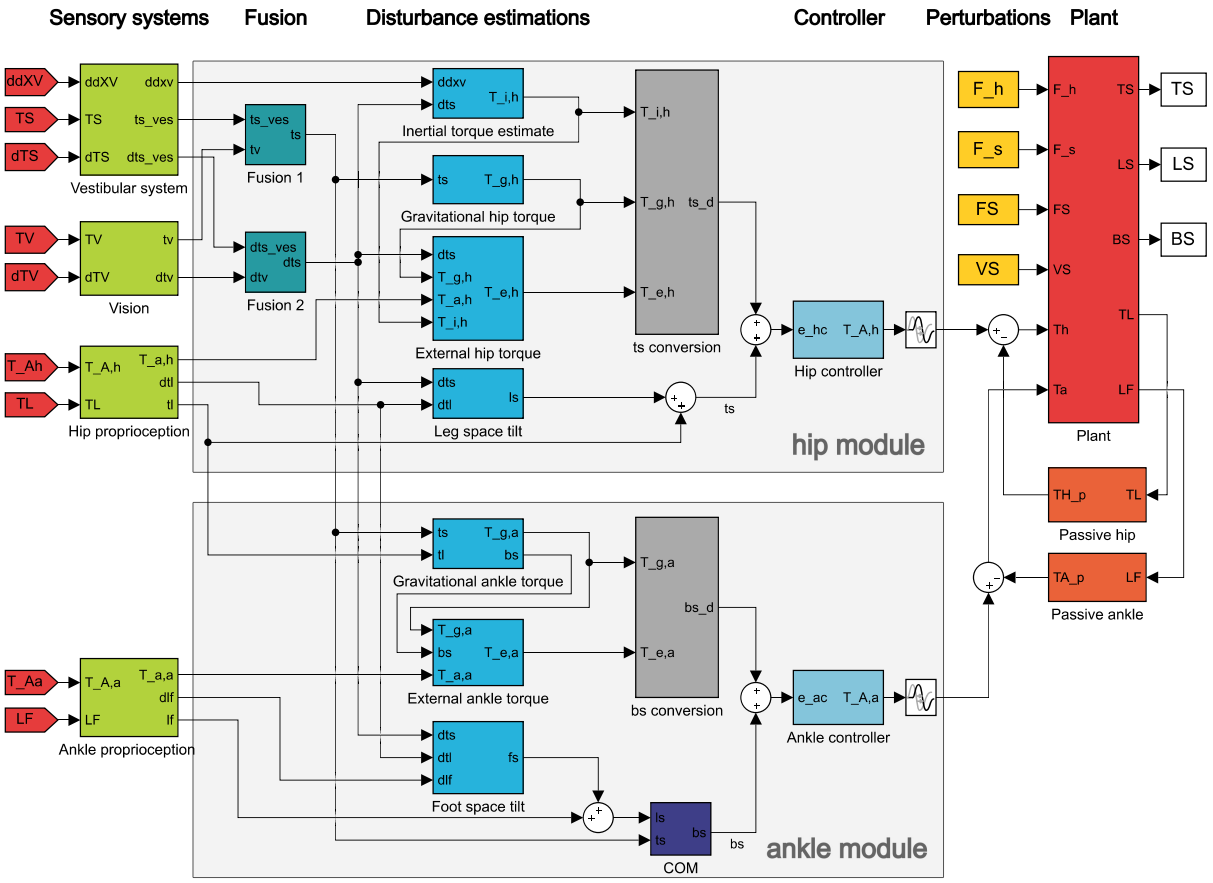

Figure 4: Overview of the DEC model that was used in this study. Signals of physical variables, originating from the plant, enter the control loop through the sensory systems. The fusion level fuses the sensory signals of the vestibular and visual system. The seven disturbance estimations are made by combining different sensory signals. The leg and foot space tilt estimates contain a gain and threshold. The grey conversion boxes contain the gains and thresholds of the torque estimates and convert the torques into angle equivalents. In the COM block, the estimated angles of the trunk and leg segments are combined to estimate the horizontal position of the COM of the whole body. The hip controller is a proportional-derivative (PD) controller that controls the COM of the trunk on top of the hip joint. The ankle module controls the COM of the whole body. The time delays represent the total neural time delays of the balance control system.

represented in lowercase letters. The sensory fusion level, in detail explained in Section II-B2, is an extra level that combines the vestibular and visual trunk angle signals and makes a visual disturbance estimation. The sensory signals are combined to form a meta level, in which seven disturbance estimations are made. Balance is controlled through two separate control loops, the hip module and the ankle module. The hip module controls the trunk angle on top of the hip joint and the ankle module controls the combined COM of the leg and trunk segments (BS) on top of the ankle joint. The three hip torque estimates are converted to ts angle equivalents by scaling the torques with a factor $1/(m_t \cdot g \cdot h_t)$ and the leg space tilt estimate is summed with the hip angle to form a ts signal equivalent to the total effect of all estimated disturbances. The sum of the four angles is the error signal for the hip controller. Equivalently, the two torque estimates of the ankle module are transformed into their angle equivalents by scaling them with the factor $1/(m_b \cdot g \cdot h_b)$ and summed with a bs estimate to form the error signal of the ankle controller. Both hip and ankle controllers are proportional-derivative (PD) controllers. The resulting active torques are delayed to represent the total neural time delays present in the balance control system. The active torques are summed with the passive torques resulting from the intrinsic muscle properties. The plant transforms the torques and applied disturbances into movement by means of the TMT method [23]. In this study, the dynamics were

not linearized, in contrast to the dynamics in the earlier presented multisegmental DEC model [20].

2) Visual disturbance estimation: Only one DEC model had been published that incorporates visual information in the model structure [19]. The published model is a single segment model that incorporates visual information only in the absence of visual disturbance. In the absence of visual disturbance, visual and vestibular systems provide the same information, which is the trunk angle relative to space (ts_{vis} and ts_{ves}). In this case, simple fusion can be done by taking a (weighted) average of the two signals [19]. When a visual disturbance is present, the visual system is not able to determine the trunk in space angle, but instead measures the trunk angle relative to the visual screen angle (tv). The vestibular and visual systems both provide the balance control system with a proportional signal, ts_{ves} and tv respectively, and a derivative signal, $\dot{ts}_{ves}$ and $\dot{tv}$ respectively. Fusion of vestibular and visual signals including calculation of the visual disturbance estimation happens before calculation of the other disturbance estimations (Fusion 1 and Fusion 2 in Figure 4). This is done because the trunk angle estimation ts is used for 5 of the 7 remaining disturbance estimations. The design of the sensory fusion, Fusion 1 in Figure 4, is shown in Figure 5. Fusion of the derivative signals in Fusion 2 in Figure 4 is done in the same way, with its own weighting factor, W_{f2}, and detection threshold, T_{f2}.

3) Model structure: An important change in the model structure is the position of the gains, thresholds and low-pass filters of the disturbance estimations. The model structure has been changed so that the disturbance estimations are modified after instead of before they are used for other disturbance estimations. Practically, this means that the gains and thresholds are applied in the grey ts and bs conversion boxes in Figure 4. This change was made to make the external torque estimates more accurate. In the absence of a visual disturbance, all sensory input is assumed to be accurate. The accurate sensory signals are used to calculate the disturbance estimations. Calculation of the disturbance estimations is therefore also accurate (up to the small angle approximations used) before scaling and thresholding takes place. External torque estimates are made by calculating the total torque from the angular accelerations and subtracting all known torques. In the model published in [20], the modified signals are used to calculate the external ankle torque estimate (external hip torque is not present). The consequence is that the external torque signal is highly dependent on the gain and threshold value of the gravitational and inertial torque estimates, resulting in an unreliable external torque signal when the gains of

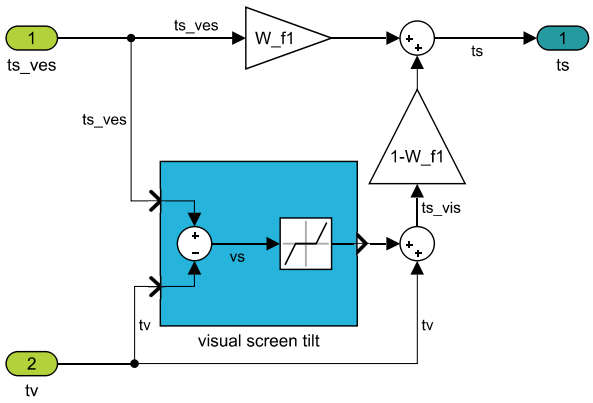

Figure 5: Fusion of the vestibular and visual information. An estimate of the visual screen tilt vs is made by taking the difference between ts_{ves} and tv, and is used to determine if the visual information is reliable. When vs is small, it is seen as noise and the signals are fused. When the vs is above the detection threshold, tv is largely attenuated. W_{f1} can be used to favour the ts_{ves} signal in the presence of a visual disturbance. In the absence of a visual disturbance, the visual signal is less noisy than the vestibular signal and the visual signal should be favoured slightly [24], [25].

the gravitational and inertial torque estimates are low and/or the thresholds are high. The model presented in this study uses the unmodified signals to calculate the external torque estimates, resulting in more accurate estimations of the external torque. This makes the external torque estimates more similar to the other disturbance estimations, where the estimates are accurate until scaling, thresholding and filtering take place.

In the presence of visual disturbance sensory signal of ts resulting from the fusion is not fully accurate, and therefore also the disturbance estimations are also somewhat inaccurate. However, using the unmodified disturbance estimation signals for the calculation of the external torque estimates will still result in a much more accurate estimate than when the signals are used that have been passed through a gain and threshold.

4) External ankle torque estimate: The external ankle torque estimate, shown in Figure 6, was already present in the DEC model published in [20], although there it is used to calculate the internal reaction force caused by the trunk segment acceleration instead of calculating an actual external torque. In our model, an external force is applied to the hips. Because of the way the external torque is calculated, it is not possible to determine the contributions of the internal reaction torque and the external ankle torque separately. Therefore the external ankle torque estimate is used to calculate the sum of the two.

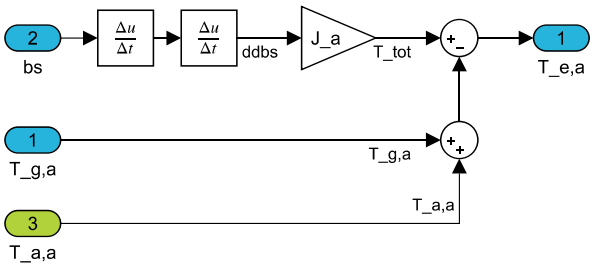

Figure 6: Calculation of the external ankle torque. The calculation is done by determining the total ankle torque from the angular acceleration of the body and subtracting all other estimated torques.

5) External hip torque estimate: The external hip torque estimate, shown in Figure 7, was added to the hip module to make the model fit conditions where an external force is applied to the trunk segment. Apart from the position of the gain, threshold and filter, the external hip torque is calculated in the same way as the external ankle torque estimate in the model presented in [20].

In summary, the multisegmental DEC model was improved with five elements. Vision was added, including a visual disturbance estimation, an external hip torque estimate was added, the external ankle torque is now the sum of the external ankle torque and the internal reaction torque, and lastly, the position of the gains and thresholds was changed. A fitting procedure was developed to fit and validate the model.

C. Fitting procedure

The model was fitted on several different signals. The basic procedure was the same for all fits and is shown in Figure 8. With this fitting procedure, the first task was to find a base set of parameters which

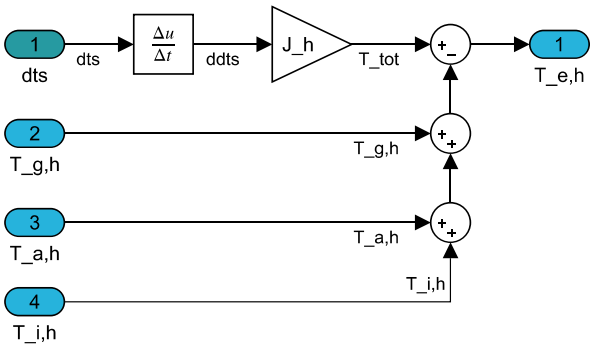

Figure 7: Calculation of the external hip torque estimate. Calculation of the external hip torque is done in the same way as the calculation of the external ankle torque.

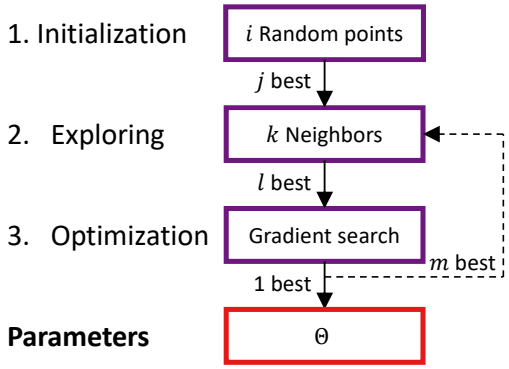

Figure 8: Flow scheme of the fitting procedure. The fitting procedure always consists of three phases. The initialization phase searches for parameters that produce stable and realistic simulation. In the exploring phase, the neighbourhood of the j best points is searched. The l best points serve as starting points for l gradient searches in the optimization phase. The gradient search that results in the best fit produces the final parameter vector Θ, or the m best results can serve as starting points for a new exploring phase.

produces stable and realistic behaviour, because it was found that the parameter values used in [20] were not able to keep the improved model upright. With a working model and a base set of parameters, three types of simulations were done:

- Fitting the model to experimental data,
- fitting the model to its own simulated data, and
- a sensitivity analysis.

The procedure consists of three phases: Initializing, exploring and fitting. Because there are so many variables, it was not feasible to perform full grid searches. Also because of the structure of the model, a large interdependence of the varied parameters was expected, making the effective parameter space dimensions smaller than the number of parameters. Therefore it was chosen to search randomly, choosing random points in the parameter space between set boundaries.

1) Initialization: In the initialization phase, the search for the right area within the parameter space was done. This was done by selecting i points in the parameter space, where every parameter had a random value between 70% and 130% of the starting point value. The initialization could be repeated several times. An error function determined which parameter set resulted in the best fit. The j best parameter sets served as starting points for the exploring phase.

2) Exploring: In the exploring phase, the neighbourhood of the j best parameter sets was searched. For each starting point, k neighbours were selected in the same way as in the initialization phase. The l best

parameter sets were determined with an error function, which could be the same or different from the error function used in the initialization phase.

3) Optimization: The l best parameter sets served as starting points for gradient searches. All gradient searches had a maximum of 200 function evaluations. The error function that was used in the exploring phase was used to select the final parameter set Θ, which was the parameter set that produced the best fit. The m best results could also serve as starting points for a new exploring phase.

D. Starting point search

Finding a working operating point for the extended model was done by first simulating the model with only the base plate rotation signal, FS, with the largest amplitude. All other perturbation signals were turned off. The largest FS amplitude was chosen because in this condition the influence of FS on the body sway is largest, thus the effect of the remaining three disturbance signals in the experimental data, which were left out in the simulations, is relatively low. Simulations were done for 8 perturbation repetitions.

To find a stable operating point of the model, 31 of the parameters present in the model were chosen to vary. These parameters include the 22 fitted parameters given in Table AI plus the 9 gains, thresholds and cutoff frequencies of the Butterworth filters (listed in Table AII) that are fixed in a later stage. Only the mechanical parameters, such as subject weight and height, listed in Table AIII, and the passive joint stiffness and damping in Table AII were fixed.

Initialization was done with $i = 2000$ random points, with boundaries of 50% lower and higher than the starting values, which were empirically found by starting with the values presented in [20] and altering them until the model could recover from a small impulse force.

The points that resulted in a stable simulation were scored with an error function based on the total variance accounted for (VAF). The VAF is a measure to quantify the quality of a non-linear model, expressed in percentages, given by

$$\text{VAF} = 1 - \frac{\sum_{k=1}^{N} \left(\hat{\boldsymbol{y}}(\boldsymbol{t}) - \boldsymbol{y}(\boldsymbol{t})\right)^2}{\sum_{k=1}^{N} \left(\boldsymbol{y}(\boldsymbol{t})\right)^2}, \tag{1}$$

where $y(t)$ is the experimental signal and $\hat{y}(t)$ is the model fit of the signal. To give the points with the highest VAF the best, thus lowest, score, the sum squared error function made up of two concatenated error vectors given by

$$E_{tot} = \sum_{k=1}^{N} \boldsymbol{E}^2, \text{ where} \tag{2}$$

$$\boldsymbol{E} = \left[2 \cdot \boldsymbol{E}_{LS} \quad \boldsymbol{E}_{TS}\right], \text{ where} \tag{3}$$

$$\boldsymbol{E}_{LS} = \frac{\boldsymbol{LS}_s - \boldsymbol{LS}_e}{\boldsymbol{LS}_e}, \text{ and} \tag{4}$$

$$\boldsymbol{E}_{TS} = \frac{\boldsymbol{TS}_s - \boldsymbol{TS}_e}{\boldsymbol{TS}_e}. \tag{5}$$

The vector $\mathbf{LS}_s$ contains the simulated LS angles over time and $\mathbf{LS}_e$ contains the measured leg angles over time of one of the experiments done with the first subject, averaged over the seven perturbation repetitions. Similarly, $\mathbf{TS}_s$ is a vector containing the simulated trunk angles and $\mathbf{TS}_e$ the experimental trunk angles over time. The vector $\boldsymbol{E}_{LS}$ in Equation 3 is weighted double to put more emphasis on the leg sway for two reasons. First, it is easier to first stabilize the lower segment and later stabilize the trunk on top of the stabilized hip joint. Second, FS is expected to have the most influence on the leg segment, along with F_h, while F_s and VS are expected to have a larger influence on the trunk segment than the support surface rotation.

The $j = 3$ best scoring points were used as starting points in the exploring phase, with $k = 1000$ neighbours. The five best points served as starting points for gradient searches using the lsqnonlin function in Matlab, using the error vector given in Equation 3, which is automatically squared by the lsqnonlin algorithm. The best scoring parameter sets, the sets with the smallest error vectors, served as starting points for new neighbour searches, with $k = 1000$, with parameter values between 70% and 130% of the given parameter starting point. This procedure was repeated several times. With FS disturbance only, the model could fit around 50% of the leg segment sway.

The second perturbation that was added to the simulations was F_h. The three best scoring parameter sets resulting from the FS-only simulations served as starting points from which the same procedure was followed. In the same way, F_s was added to the simulations after the best scoring points of the simulations containing FS and F_h were found. The error vector was now changed to

$$\boldsymbol{E} = \left[\boldsymbol{E}_{LS} \quad \boldsymbol{E}_{TS}\right], \tag{6}$$

because with already stable LS sway and with the shoulder perturbation present, the emphasis on LS was no longer desired. Lastly, VS was added using the same procedure and with the error shown in

Equation 6. Model fits with VAFs of around 60% for both segments were found in this way.

E. Model fits to experimental data

The model was fitted to the experimental data of 6 random subjects. For each subject, one parameter set was fitted to the experimental data in the three conditions. The model simulations consisted of 8 perturbation repetitions. The responses, TS and LS, averaged over the perturbation repetitions, served as the fitted signals. The 22 fitted parameters were the two weighting factors and thresholds of the fusion, and the gains and thresholds of all seven disturbance estimations (Table AI). Each fitting has the same parameter set as basis. With this parameter set, initialization was done with $i = 1000$ random values between 70% and 130% of the starting value for all parameters. Each starting point was given a VAF-based sum squared error vector (Equation 2) made up of the concatenated error vectors of three simulations in the different conditions. The concatenated error vector is given by

$$\boldsymbol{E} = [\boldsymbol{E}_{low} \quad \boldsymbol{E}_{med} \quad \boldsymbol{E}_{high}] \,, \tag{7}$$

where $\boldsymbol{E}_{low}$, $\boldsymbol{E}_{med}$ and $\boldsymbol{E}_{high}$ are the error vectors given by Equation 6 of the three conditions.

Exploring was done with $k = 1000$ neighbours of the $j = 1$ best scoring parameter set and boundaries between 70% and 130%. With the $l = 5$ best scoring points as starting points, five gradient searches were done with the error vector given in Equation 7. For both the random search and the gradient search, lower boundaries were applied, making sure parameter values did not become negative.

F. Model fits to simulated data

To determine how well the model parameters are able to fit, the model was also fitted to simulated data. To create the simulated "experimental" data, the model was simulated with the parameter set that resulted in the highest VAF with experimental data. This was done three times, with the parameter sets corresponding to the model fits to experimental data of three subjects. The same fitting procedure was used as for the experimental data. No noise was added to the simulated "experimental" signals to eliminate unwanted extra effects.

G. Sensitivity analysis

A sensitivity analysis was done to test the robustness of the model against measurement and estimation errors of the biomechanical parameters. The sensitivity analysis was done by taking the parameter set resulting from the fitting of the model to the experimental data of subject 1 as the base parameter set. The model was simulated twice for each biomechanical parameter. Each biomechanical parameter (Table AIII) was once decreased and once increased with 10%, while all other parameters were kept the same. The amount of influence of the parameter change on the simulation was calculated using the ΔVAF, which is defined as

$$\Delta\text{VAF} = \text{VAF}_p - \text{VAF}_O \,, \tag{8}$$

where VAF_p is the VAF of the simulation on the experimental data with one parameter increased of decreased, and VAF_O is the VAF of the original simulation on the experimental data of subject 1. The model was simulated in all three conditions, and for both segment signals, the average ΔVAF was taken over all three conditions.

III. Results

A. Model fits to experimental data

To get a general idea of what the experimentally measured sway signals and the fitted sway signals look like, the signals of a representative subject are shown in Figure 9. The figure shows the model fit loosely following the experimental signal but not being able to reproduce all signal behaviour. For example, the experimental LS signal shows an angle of about $1\,\text{deg}$ after about 3 seconds in all conditions, but the model is not able to reproduce this LS sway peak in any of the conditions.

To investigate the experimental and simulated behaviour in more detail, a zoomed-in view of the signals of a representative subject is shown in Figure 10. The figure shows that for both the experimental and simulated signals, the differences between the three conditions are small. The figures indicate that for both the experimental and the simulated signals the difference in behaviour between the different conditions lies mainly in the lowest frequencies, while the higher frequencies, which show oscillating-like behaviour, are quite similar over the three conditions. The same holds for the differences between the experimental signals and the fitted signals. The difference between the experimental signals and the simulated signals is largely present in the low frequencies, while the higher frequencies are fitted quite well by the model. Also, the highest, noisy-like frequencies are not present in the simulations.

The parameter search for realistic model behaviour resulted in a set of fixed parameter values, listed in Table I, and a set of starting values for the fitted parameters, listed in Table IIa. Table IIa also lists the

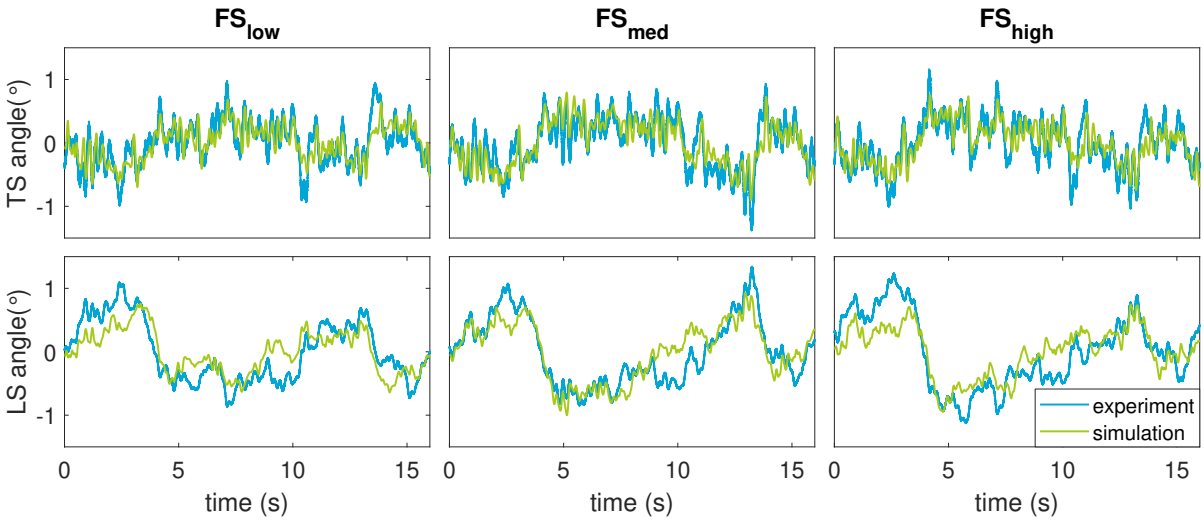

Figure 9: Angles of the trunk segment (top) and leg segment (bottom) over time for subject 1 in the three different conditions. The experimental signals are the average of 7 consecutive perturbation periods. The simulation was fitted to maximize the VAF between the experimental sway and simulated sway.

values of the fitted parameters that resulted from the fitting of the model to the experimental data of the six subjects, as well as the mean values and standard deviation for each parameter. A number of parameters show a large standard deviation, indicating a large variance between the different subjects. Furthermore, the time delays, td_h and td_a, are consistently fitted extremely small.

Fitting the model to experimental data resulted in six VAFs per subject, two for each of the three conditions, one for the TS signal and one for the LS signal. The six VAFs for each subject, and the mean VAF of LS and TS for each subject are listed in Table IIb. For some subjects, the model simulations fitted better than for others, resulting in differences in the mean VAFs per subject of about 10%. But also within subjects, there are differences in the quality of the fit in the different conditions. For almost all subjects, the FS_{med} condition is fitted best. Lastly, for some subjects, one of the two body segments was consistently better fitted by the model than the other, in all conditions.

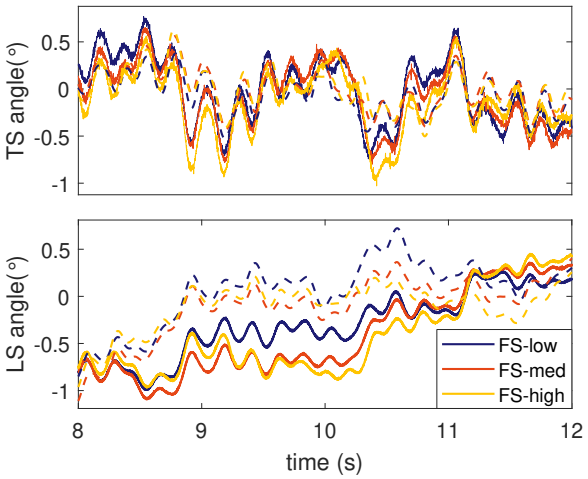

Figure 10: Sway signals of the trunk segment and leg segment of subject 4. The experimental signals (solid lines) and fitted signals (dashed lines) for the three different conditions are shown within a 4 second time frame.

B. *Model fits to simulated data*

When the model was fitted to simulated data, the fit always converged, resulting in VAFs $> 99.5\%$ for every signal for all subjects. Of the 22 fitted

Table I: Values of the fixed parameters. The list of parameter abbreviations is given in Table AII.

Parameter	Value
$F_{i,h}$ (rad/s)	2
$F_{p,h}$ (rad/s)	0.01
$F_{e,h}$ (rad/s)	2
$F_{p,a}$ (rad/s)	0.01
$F_{e,a}$ (rad/s)	2
$k_{p,h}$ (Nm/rad)	$0.15 \cdot m_t g h_t$
$k_{d,h}$ (Nm s/rad)	$0.03 \cdot m_t g h_t$
$k_{p,a}$ (Nm/rad)	$0.15 \cdot m_b g h_b$
$k_{d,a}$ (Nm s/rad)	$0.045 \cdot m_b g h_b$
$K_{p,h}$ (Nm/rad)	$1.5 \cdot m_t g h_t$
$K_{d,h}$ (Nm s/rad)	$0.3 \cdot m_t g h_t$
$K_{p,a}$ (Nm/rad)	$1.5 \cdot m_b g h_b$
$K_{d,a}$ (Nm s/rad)	$0.3 \cdot m_b g h_b$

Table II: **a.** The values of the fitted parameters of the starting point and for the fits to the experimental data of six subjects, including the mean and standard deviation for each parameter. The list of parameter abbreviation is given in Table AI. **b.** VAFs of the model fits to the six different signals for each subject, including the means per condition and per body segment.

a.

		Subject						
Param.	**Start**	**1**	**2**	**3**	**4**	**5**	**6**	**Mean (std)**
W_{f1}	0.995	1.00	1.00	0.994	0.903	1.00	0.997	0.98 (0.036)
T_{f1} (rad)	0.00196	0.0230	0.0268	0.00136	0.00469	0.00252	0.00237	0.010 (0.011)
W_{f2}	0.768	0.861	1.00	0.647	0.999	1.00	1	0.92 (0.13)
T_{f2} (rad/s)	0.00130	0.00974	1.57e-6	0.00227	7.94e-6	0.0475	6.29e-7	0.010 (0.017)
$G_{i,h}$	0.0941	0.0858	0.283	0.170	0.337	0.190	0.394	0.24 (0.10)
$T_{i,h}$ (Nm)	0.00696	0.0911	0.0291	0.00421	0.0999	0.0394	3.70e-4	0.044 (0.039)
$G_{g,h}$	0.967	0.928	0.182	0.544	0.200	6.28e-6	0.626	0.41 (0.32)
$T_{g,h}$ (Nm)	0.0165	0.00841	0.00446	8.82e-4	0.00804	0.0948	0.00364	0.020 (0.034)
$G_{p,h}$	0.131	0.0332	0.00292	0.00221	0.019	1.00	0.00399	0.18 (0.37)
$G_{e,h}$	0.154	0.178	0.752	0.327	0.608	0.00156	0.611	0.41 (0.27)
$T_{e,h}$ (Nm)	0.00470	0.0947	0.0871	0.068	6.01e-5	0.0973	0.0988	0.074 (0.035)
G_{ls}	2.39	1.97	1.48	1.62	1.40	1.45	2.01	1.7 (0.25)
T_{ls} (rad/s)	5.94e-4	1.73e-5	0.00113	0.00289	4.75e-4	3.57e-5	0.0164	0.0035 (0.0059)
$G_{g,a}$	0.975	1.18	0.911	0.921	0.647	0.607	0.579	0.81 (0.22)
$T_{g,a}$ (Nm)	0.0225	1.24e-4	5.83e-4	0.00390	0.093	0.0166	0.0294	0.024 (0.033)
$G_{p,a}$	6.16e-4	0.00454	0.0103	0.240	1.54e-4	0.0172	5.53e-7	0.045 (0.087)
$G_{e,a}$	0.748	0.834	0.846	0.586	0.530	0.586	0.541	0.65 (0.13)
$T_{e,a}$ (Nm)	0.00183	0.0250	0.0197	1.09e-5	1.13e-4	0.0754	0.0994	0.037 (0.038)
G_{fs}	1.88	2.21	2.30	2.32	2.31	1.82	1.75	2.1 (0.24)
T_{fs} (rad/s)	0.0988	0.138	0.148	0.150	0.148	0.100	0.0872	0.13 (0.025)
td_h (s)	0.0349	0.0303	0.0359	0.0328	0.0406	0.0477	0.0481	0.039 (0.0069)
td_a (s)	0.0823	0.0576	0.0502	0.0674	0.0534	0.0556	0.0789	0.061 (0.010)

b.

Condition	**Signal**	**1**	**2**	**3**	**4**	**5**	**6**	**Mean**
$\mathbf{FS_{low}}$	LS	62,8%	56,6%	41,0%	45,3%	50,3%	49,8%	51,0%
	TS	60,5%	44,9%	61,6%	49,0%	46,3%	50,8%	52,2%
	Mean	61,7%	50,8%	51,3%	47,2%	48,3%	50,3%	51,6%
$\mathbf{FS_{med}}$	LS	72,4%	70,6%	65,9%	58,5%	73,7%	61,1%	67,0%
	TS	67,6%	44,0%	61,1%	54,2%	49,5%	61,1%	56,3%
	Mean	70,0%	57,3%	63,5%	56,4%	61,6%	61,1%	61,6%
$\mathbf{FS_{high}}$	LS	68,7%	68,5%	57,8%	51,5%	49,5%	59,8%	59,3%
	TS	65,5%	44,3%	66,4%	49,2%	55,2%	64,7%	57,5%
	Mean	67,1%	56,4%	62,1%	50,4%	52,3%	62,2%	58,4%
Mean	LS	68,0%	65,2%	54,9%	51,8%	57,8%	56,9%	59,1%
	TS	64,5%	44,4%	63,0%	50,8%	50,3%	58,9%	55,3%
	Mean	66,3%	54,8%	59,0%	51,3%	54,1%	57,9%	57,2%

parameters, 13 converged to a value within 5% of deviation of the correct value. Of the remaining 9 parameters, the parameters that converged to a value larger than 5% deviant from the correct value of at least one of the five gradient searches, the values are plotted in Figure 11. For increased visibility, the values were normalized with the experimental value, so a value of 1 means that the estimate is correct. The figure shows that some parameters are consistently estimated several factors too large or too small. The figure also shows that the fourth gradient search, which converged slower than the other four gradient searches by coincidence, estimates the parameters visibly worse for at least five of the parameters, though the VAF is only 0.10% lower than that of the other four gradient searches.

C. Sensitivity analysis

To test the model's robustness against imprecise measurements and estimations of the biomechanical parameters, a sensitivity analysis was done. The average ΔVAF of the trunk segment sway and leg segment sway over three conditions is given in Figure 12. For the trunk segment sway, the most influential biomechanical parameters are the trunk mass (m_t), the COM height of the trunk (h_t) and moment of inertia of the body around the ankle (J_a), all resulting in a ΔVAF in the order of 1%. For the leg sway, most parameters have even less influence on the fit. All ΔVAF values are smaller than 0.7% for the leg segment signals.

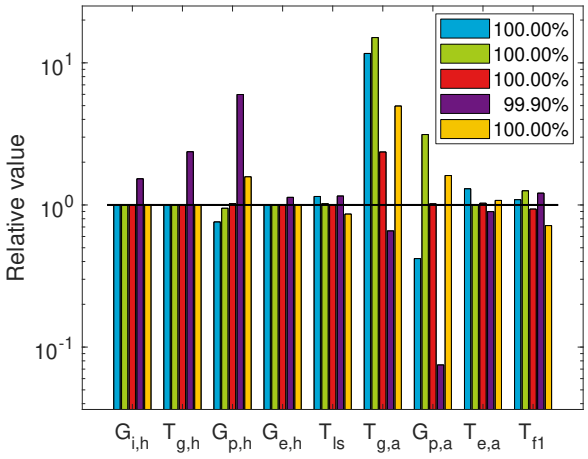

Figure 11: The resulting VAFs and normalized parameter values of the five gradient searches of the fitting on the simulated data of subject 1 are shown. Only 9 out of 22 are shown, the parameters that fitted within 5% smaller or larger than the simulation value for all five fits were left out.

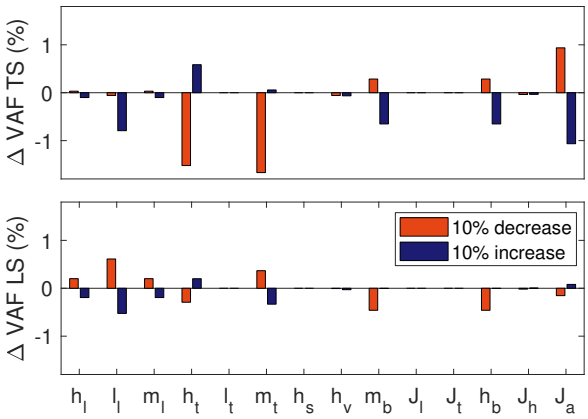

Figure 12: The change in variance unaccounted for (ΔVAF) of the simulation when each biomechanical parameter is decreased or increased by 10%, compared to the simulation with the unchanged parameters.

IV. Discussion

The goal of this study was to investigate to what extent the multisegmental DEC model is able to fit to the experimental data containing multiple sensory and mechanical disturbances. To this aim, the multisegmental DEC model was extended and its ability to describe experimental data of subjects enduring multiple disturbances in multiple conditions was investigated.

The results presented in Table IIb and Figure 9 show that the extended DEC model was able to balance itself in the applied conditions. More importantly, the model is able to capture important aspects of human balance in these conditions. With only one set of parameters per subject, the model was able to fit to experimental data in three different conditions for all subjects, obtaining a VAF between 40% and 70% for all individual signals and obtaining an average VAF of around 57%. Figure 10 shows that the higher frequencies are fitted quite well, while the fit is worse for the lower frequencies.

The results in Table II show that the parameter estimations are quite divergent. Some parameters, such as $G_{p,h}$ and T_{f2}, show large differences in estimated values between subjects. Although differences between subjects are expected, it is not likely that, for example, subject 1 uses the gravitational hip torque estimate for 100%, while subject 5 almost completely ignores the signal ($G_{g,h}$ in Table IIa). Other parameters are consistently estimated too high or too low. For example, time delays td_h and td_a are consistently estimated smaller than physiologically possible [26]. These results indicate that parameter estimation of the model is still a challenge.

A comparison of the five gradient searches of the model fits to simulated data, in Figure 11, shows that a small difference in the quality of the fit can be caused by a large difference in parameter values. The figure shows that even if only 0.1% of the variance is not captured by the model, some parameter values can be estimated over a factor 10 too small or too large. These findings indicate that small improvements in model fits to experimental data could lead to bigger improvements in parameter estimation for some parameters.

A. Scientific importance

A big strength of this study lies in the combining of neurological knowledge and engineering tools. For the first time, a model with a strong neurological foundation has been applied to an advanced experimental data set designed for system identification. To that aim, an extensive multisegmental DEC model was developed, making the multisegmental DEC model more widely applicable to even the most advanced experimental setups used in balance control research. The model structure has also been improved by reducing the interdependence of the disturbance estimates and related parameters.

Analysis of the DEC model simulations has been improved as well, by which more insight into the working of the DEC model was gained. Analysis of the model was fully done in the time domain. Because the model is non-linear, commonly used analysis methods in the frequency domain, as done in [20], cannot be applied without obtaining biased results. Therefore comparing the results obtained with the DEC model

presented here with the earlier published model poses a problem. Because of the non-linearities in the model, it is possible that the applied methods of analysis have not been used correctly and the results presented in [20] paint a more positive picture than the reality. By doing the analysis in the time domain, such biases have been eliminated, although the use of sophisticated frequency analysis methods for non-linear systems could add value.

Lastly, the sensitivity analysis of the developed DEC model to the biomechanical parameters has proven the model's robustness against errors and inaccuracies in the measurements and estimations of the biomechanical parameters. The sensitivity analysis also confirms that the fits have not yet reached the local or global minimum after the fitting procedure, because decreasing or increasing parameters sometimes leads to better fits for both segments.

B. Limitations

Many limitations of this study can be traced back to one cause, which is the amount of time and computational power that was available. All choices in the fitting procedure were made based on a trade-off between time efficiency and the quality of the results. A total of 49 parameters determine the behaviour of the model, of which only a few can be measured or reliably estimated in advance. With the time and computational power that was available, it was not possible to systematically search the parameter space of the remaining parameters by means of a grid search to get a global idea of the error landscape. When looking only at the 22 fitted parameters, even a grid with a resolution of two values per parameter would have required 2^{22} function evaluations. And with a simulation rate of approximately 10 function evaluations per minute that would equal a total simulation time of roughly 10 months. Therefore, operating points had to be found randomly, making the found parameter values somewhat arbitrary and making the experiment difficult to repeat.

The visual information that was added to the model had some unexpected results. The estimated values of the weighing factors W_{f1} and W_{f2} suggest that the visual information is almost completely ignored in the present conditions with the visual disturbance. From literature though, we know that visual disturbance does have an influence on human balance [11], [13]. This indicates that the model is not yet able to capture the effect that the visual disturbance has on human balance.

When the model is applied to the BalRoom data set, gains and thresholds of the disturbance estimations vary widely, often approaching the lower limit or exceeding the theoretical upper limit when allowed. It appears that the disturbance estimations of segment orientations are favoured over torque estimates. For example, the gains G_{ls} and G_{fs} are always higher than the theoretical upper limit of 1, and gains such as $G_{i,h}$ and $G_{g,a}$, that rarely exceed the theoretical upper limit, but often approach the lower limit of 0. These results indicate that the way in which disturbance estimations are calculated and used can still be improved.

Thresholds show an equal amount of variance. For some thresholds, such as $T_{i,h}$ and $T_{e,a}$, this can possibly be explained by the effect of the low pass filters that are applied to the signals after the thresholds. The low pass filters have a low cutoff frequency compared to the filters used in [20], eliminating a large amount of high-frequency behaviour. Because the thresholds have a similar function of eliminating high frequencies, regarded as noise, it is possible that their function is partially taken over by the filters. Additionally, the low gains preceding some of the thresholds suggest that the signal is almost completely ignored, thus in these cases the value of the threshold is expected to have little influence on the model behaviour.

C. Future work

The DEC model was designed from a neurological perspective. A large number of parameters are present in order for the model to represent known and hypothesized neurological aspects of human balance control. Redundancy in the model and in the parameters is therefore inevitable. However, the redundancy makes fitting difficult. The nature of the closed loop control system makes it difficult to determine how the parameters influence each other. If more time and computational power are available, a more extensive investigation into the parameters space could reveal some interdependences and could gain more insight into the behaviour of the model in the applied experimental conditions.

A suggested improvement, that is easily made is and improves redundancy as well as computation time, is fixing $G_{p,h}$ and $G_{p,a}$. The parallel low pass component of the gravitational torque estimates have the mere purpose of preventing the subject from falling over due to very low frequencies over a long time and are not expected to have a large influence on the model behaviour. By fixing the gains on a value that is expected, around 0.1 or 0.15, the parameters space that has to be searched is decreased from 22 to 20 dimensions. Fixing the low pass component also reduces the amount of redundancy in the fitted parameters. For subject 5 $G_{g,h}$ was fitted to a value of

almost 0, while $G_{p,h}$ is 1, indicating that the low pass component took over the function of main gravitational torque estimate signal, which is not desirable. With fixed low pass gains, this would not happen and the model is expected to behave more in the way it was designed.

The model that was presented in Chapter II was largely based on the model presented in [20]. However many additions and adaptations were done to the model. Visual information was added, which had only been done before in a single-segment DEC model [19], and a visual disturbance estimation was created to deal with the effect of the visual screen tilt in the experimental data. An external torque estimate was added to the hip module to deal with the pusher to the hips. Furthermore, the external torque estimate in the ankle module is now actually used to estimate an external torque instead of estimating internal reaction forces. The model structure was also changed so that the external estimate is not anymore dependent on the gains and thresholds of the other disturbance estimates in the hip module.

All adaptations to the existing DEC model were made simultaneously, because the nature of the available experimental data did not allow for the changes to the model to be made one by one. Therefore, it was not possible to investigate the influence of each adaptation separately. It would be a huge improvement to add each new or adapted feature of the model separately and analyze the effect thoroughly before adding the next feature. To do this, a broader experimental data set is necessary, in which subjects are also subjected to a subset of perturbations at once. The desired data set would contain trials in which each perturbation signal is applied separately, while the remaining three perturbations are turned off, and combinations of two or three perturbations. With the extended data set, each element can be added separately while validating the adaptation with experimental data before adding the next.

V. Conclusion

In this study, an extensive multisegmental DEC model was developed. The model has a strong physiological foundation and is able to perform sensory reweighing implicitly, meaning that only one set of parameters can describe human balance in multiple conditions. Both features make the multisegmental DEC model a good candidate for diagnostic purpose in balance impairment.

The model was put to trial by fitting model simulations to one of the most challenging data sets available, of humans enduring visual, proprioceptive and two mechanical disturbances all at once in the BalRoom. With only limited time and computational power, the DEC model was already able to fit up to 70% of the experimental behaviour, showing that the model has much potential for improvement with more available resources.

With the development of a complete multisegmental DEC model and the application of the model to the BalRoom data set, a big step towards diagnosing underlying cause of balance impairment has been made. With the proposed improvements, the diagnosis of balance impairment could be possible in the near future, allowing for better treatment and quality of life in patients.

References

[1] J. H. Pasma, D. Engelhart, A. C. Schouten, H. van der Kooij, A. B. Maier, and C. G. Meskers, "Impaired standing balance: The clinical need for closing the loop," *Neuroscience*, vol. 267, pp. 157–165, 2014.

[2] L. W. Chu, I. Chi, and A. Y. Chiu, "Incidence and predictors of falls in the Chinese elderly," *Annals of the Academy of Medicine Singapore*, vol. 34, no. 1, pp. 60–72, 2005.

[3] H. Luukinen, K. Koski, L. Hiltunen, and S. L. Kivelä, "Incidence rate of falls in an aged population in Northern Finland," *Journal of Clinical Epidemiology*, vol. 47, no. 8, pp. 843–850, aug 1994.

[4] K. Rapp, E. Freiberger, C. Todd, J. Klenk, C. Becker, M. Denkinger, C. Scheidt-Nave, and J. Fuchs, "Fall incidence in Germany: results of two population-based studies, and comparison of retrospective and prospective falls data collection methods," *BMC Geriatrics*, vol. 14, no. 1, p. 105, 2014.

[5] P. A. Stalenhoef, J. P. M. Diederiks, L. P. De Witte, K. H. Schiricke, and H. F. J. M. Crebolder, "Impact of gait problems and falls on functioning in independent living persons of 55 years and over: A community survey," *Patient Education and Counseling*, vol. 36, no. 1, pp. 23–31, jan 1999.

[6] S. R. Cummings, J. L. Kelsey, M. C. Nevitt, and K. J. O'DOWD, "Epidemiology of osteoporosis and osteoporotic fractures," *Epidemiologic reviews*, vol. 7, no. 1, pp. 178–208, 1985.

[7] I. D. Loram and M. Lakie, "Direct measurement of human ankle stiffness during quiet standing: The intrinsic mechanical stiffness is insufficient for stability," *Journal of Physiology*, vol. 545, no. 3, pp. 1041–1053, dec 2002.

[8] T. Mergner, C. Siebold, G. Schweigart, and W. Becker, "Human perception of horizontal trunk and head rotation in space during vestibular and neck stimulation," *Experimental Brain Research*, vol. 85, no. 2, pp. 389–404, 1991.

[9] F. B. Horak, C. L. Shupert, and A. Mirka, "Components of postural dyscontrol in the elderly: A review," pp. 727–738, 1989.

[10] T. Muehlbauer, C. Besemer, A. Wehrle, A. Gollhofer, and U. Granacher, "Relationship between strength, power and balance performance in seniors," *Gerontology*, vol. 58, no. 6, pp. 504–512, 2012.

[11] R. J. Peterka, "Sensorimotor integration in human postural control." *Journal of neurophysiology*, vol. 88, no. 3, pp. 1097–118, sep 2002.

[12] C. D. Ford-Smith, J. F. Wyman, R. Elswick Jr, T. Fernandez, and R. A. Newton, "Test-retest reliability of the sensory organization test in noninstitutionalized older adults," *Archives of physical medicine and rehabilitation*, vol. 76, no. 1, pp. 77–81, 1995.

[13] J. H. Pasma, D. Engelhart, A. B. Maier, R. G. K. M. Aarts, J. M. A. van Gerven, J. H. Arendzen, A. C. Schouten, C. G. M. Meskers, and H. van der Kooij, "Reliability of System Identification Techniques to Assess Standing Balance in Healthy Elderly." *PloS one*, vol. 11, no. 3, p. e0151012, mar 2016.

[14] D. C. Mackey and S. N. Robinovitch, "Mechanisms underlying age-related differences in ability to recover balance with the ankle strategy," *Gait & posture*, vol. 23, no. 1, pp. 59–68, 2006.

[15] C. Horlings, U. Küng, B. Van Engelen, N. Voermans, G. Hengstman, A. van der Kooi, B. R. Bloem, and J. H. Allum, "Balance control in patients with distal versus proximal muscle weakness," *Neuroscience*, vol. 164, no. 4, pp. 1876–1886, 2009.

[16] T. Mergner, "A neurological view on reactive human stance control," *Annual Reviews in Control*, vol. 34, no. 2, pp. 177–198, dec 2010.

[17] R. J. Peterka, "Simplifying the complexities of maintaining balance insights provided by simple closed-loop models of human postural control." *IEEE Engineering in Medicine and Biology Magazine*, vol. 22, no. 2, pp. 63–68, mar 2003.

[18] T. Mergner, G. Schweigart, and L. Fennell, "Vestibular humanoid postural control," *Journal of Physiology Paris*, vol. 103, no. 3-5, pp. 178–194, may 2009.

[19] L. Assländer, G. Hettich, and T. Mergner, "Visual contribution to human standing balance during support surface tilts," *Human Movement Science*, vol. 41, pp. 147–164, jun 2015.

[20] G. Hettich, L. Assländer, A. Gollhofer, and T. Mergner, "Human hip–ankle coordination emerging from multisensory feedback control," *Human Movement Science*, vol. 37, pp. 123–146, oct 2014.

[21] M. F. Folstein, S. E. Folstein, and P. R. McHugh, ""mini-mental state": a practical method for grading the cognitive state of patients for the clinician," *Journal of psychiatric research*, vol. 12, no. 3, pp. 189–198, 1975.

[22] D. A. Winter, *Biomechanics and motor control of human movement*. John Wiley & Sons, 2009.

[23] R. Q. van der Linde and A. L. Schwab, *Multibody Dynamics B*, 2011.

[24] M. Cohen, R. J. Crosbie, and L. Blackburn, *Disorienting effects of aircraft catapult launchings*. Crew Systems Department, Naval Air Development Center, 1973.

[25] T. Mergner and S. Glasauer, "A simple model of vestibular canal-otolith signal fusion," in *Annals of the New York Academy of Sciences*, vol. 871, 1999, pp. 430–434.

[26] T. Kiemel, A. J. Elahi, and J. J. Jeka, "Identification of the plant for upright stance in humans: multiple movement patterns from a single neural strategy," *Journal of neurophysiology*, 2008.

APPENDIX A
MODEL DESCRIPTION

The multisegmental DEC model consists of several levels: the sensory systems, the disturbance estimations (including the sensory fusion), the controller and the plant. The four levels are explained in detail below. The involved parameters are listed in Tables AI, AII and AIII. The physical variables that are present in the control loop are listed in Table AIV.

A. Sensors

The sensor level is where information of the state of the system enters the control loop. Information that is available to the control system is limited to the information that the sensory systems are able to measure. The sensory systems transform the physical parameters, written with capital letters, into internal signals of the neural system, written in lowercase letters. There are four sensory systems included in the model.

1) Vestibular system: The vestibular system provides the balance control system with three signals, the trunk space angle, the trunk space velocity and the horizontal acceleration of the head, ts_{ves}, $\dot{ts}_{ves}$ and $\ddot{x}_{ves}$ respectively.

Table AI: The abbreviations of the 22 model parameters that are fitted.

Fitted parameters	
Fusion 1	
Weighting factor	W_{f1}
Threshold	T_{f1}
Fusion 2	
Weighting factor	W_{f2}
Threshold	T_{f2}
Inertial hip torque estimate	
Gain	$G_{i,h}$
Threshold	$T_{i,}$
Gravitational hip torque estimate	
Gain	$G_{g,h}$
Threshold	$T_{g,h}$
Gain parallel component	$G_{p,h}$
External hip torque estimate	
Gain	$G_{e,h}$
Threshold	$T_{e,h}$
Leg space tilt estimate	
Gain	G_{ls}
Threshold	T_{ls}
Gravitational ankle torque estimate	
Gain	$G_{g,a}$
Threshold	$T_{g,a}$
Gain parallel component	$G_{p,a}$
External ankle torque estimate	
Gain	$G_{e,a}$
Threshold	$T_{e,a}$
Foot space tilt estimate	
Gain	G_{fs}
Threshold	T_{fs}
Neural time delays	
Hip module	td_h
Ankle module	td_a

Table AII: The abbreviations of the 13 fixed model parameters.

Fixed parameters	
Inertial hip torque estimate	
Cutoff frequency	$F_{i,h}$
Gravitational hip torque estimate	
Cutoff frequency parallel component	$F_{p,h}$
External hip torque estimate	
Cutoff frequency	$F_{e,h}$
Gravitational ankle torque estimate	
Cutoff frequency parallel component	$F_{p,a}$
External ankle torque estimate	
Cutoff frequency	$F_{e,a}$
Intrinsic muscle properties	
Passive hip stiffness	$k_{p,h}$
Passive hip damping	$k_{d,h}$
Passive ankle stiffness	$k_{p,a}$
Passive ankle damping	$k_{d,a}$
Controller parameters	
Hip controller proportional gain	$K_{p,h}$
Hip controller derivative gain	$K_{d,h}$
Ankle controller proportional gain	$K_{p,a}$
Ankle controller derivative gain	$K_{d,a}$

2) Vision: The visual system provides the balance control system with the angle of the trunk relative to the visual screen, tv, and the derivative of the same angle, $\dot{tv}$. In the absence of a visual disturbance, this is essentially the same information as the vestibular system provides, ts and $\dot{ts}$.

3) Hip proprioception: Hip proprioception senses the angle and change in angle between the trunk and the legs, tl and $\dot{tl}$ respectively. Additionally, the active torque around the hip caused by muscle contractions, $T_{a,h}$ is sensed by the proprioceptive system.

4) Ankle proprioception: Analogous to hip proprioception, ankle proprioception senses the angle and change in angle of the ankle, which is the angle between the feet and the legs, lf and $\dot{lf}$. Additionally the active ankle torque $T_{a,a}$ is measured.

Table AIII: The abbreviations of the 14 biomechanical model parameters.

Biomechanical parameters	
Measured parameters	
Length legs	l_l
Length head-arms-trunk (HAT)	l_t
Hip-shoulder distance	h_s
Estimated parameters	
Center of Mass (COM) height legs	h_l
COM height HAT (above hip)	h_t
Height vestibular system	h_t
Mass legs	m_l
Mass HAT	m_t
Moment of inertia (MOI) legs	J_l
MOI HAT	J_t
Calculated parameters	
Mass body	m_b
COM height body	h_b
MOI HAT around hip	J_h
MOI body around ankle	J_a

Table AIV: Physical variables that are used in the balance control feedback loop.

Physical variables	
Vestibular system	
Horizontal head accleration	ddXV
Trunk-space angle	TS
Trunk-space angular velocity	dTS
Vision	
Trunk-screen angle	TV
Trunk-screen angular velocity	dTV
Hip proprioception	
Active hip torque	T_A,h
Hip angle	TL
Hip angular velocity	dTL
Ankle proprioception	
Active ankle torque	T_A,a
Ankle angle	LF
Ankle angular velocity	dLF

B. Disturbance estimations

1) Fusion: Fusion of vestibular and visual signals including calculation of the visual disturbance estimation happens before calculation of the other disturbance estimations (see Fusion 1 and Fusion 2 in Figure 4). This is done because the trunk angle estimation ts is used for 5 of the 7 remaining disturbance estimations. The design of the sensory fusion, Fusion 1 block in Figure 4, is shown in Figure 5. Fusion of the derivative signals in Fusion 2 in Figure 4 is done in exactly the same way, with its own weighting factor, W_{f2} and detection threshold value, T_{f2}.

2) Inertial hip torque estimate: As a result of rotational acceleration of the legs, $\ddot{ls}$, there is a horizontal acceleration of the hip joint. It is assumed that the nervous system can calculate this acceleration using the $\ddot{x}_{ves}$ signal of the vestibular system and the $\dot{ts}$ signal from the fusion block, differentiated to become $\ddot{ts}$. The horizontal acceleration of the hip causes an inertial torque on the hip, caused by the inertia of the trunk segment. The resulting torque is given by

$$T_{i,h} = -m_t \cdot h_t \cdot \ddot{x}_h, \tag{9}$$

which represents the inertial force of the trunk multiplied by the distance between the hip and the COM of the trunk. The estimate $T_{i,h}$ is passed through a gain, thresholded and low-pass filtered. The low-pass filter is necessary to remove the high frequencies that result from the acceleration terms.

3) Gravitational hip torque: The Gravitational hip torque estimate is the estimate of the torque resulting from the gravitational force on the trunk. The gravitational hip torque is, using the small angle approximation of $\sin(ts) = ts$, given by

$$T_{g,h} = m_t \cdot g \cdot ts. \tag{10}$$

The signal is assumed to be split into a thresholded signal and a low-pass component that removes the very lowest frequencies.

4) External hip torque: The external hip torque estimate is used to make an estimation of the torque caused by the externally applied forces on the trunk. In this case, that is the result of the force perturbation applied to the shoulders. It takes the rotational acceleration of the trunk, calculates the corresponding net torque and subtracts all other, known, torques. The $\dot{ts}$ signal is differentiated and multiplied by the moment of inertia of the trunk around the hip joint, which is given by

$$J_{t,h} = J_t + m_t \cdot h_t^2, \tag{11}$$

resulting in the net torque in the hip joint

$$T_{tot_h} = J_{t,h} \cdot \ddot{ts}. \tag{12}$$

The external torque is calculated from all known torques by

$$T_{e,h} = T_{tot,h} - T_{g,h} - T_{i,h} - T_{a,h}. \tag{13}$$

The resulting signal is passed through a gain, a threshold, and passed through a low-pass filter.

5) Leg space tilt: The leg space estimator uses the $\dot{ts}$ signal from the fusion level and $\dot{tl}$ signal from the hip proprioception to make an estimate of the leg space tilt, by

$$\dot{ls} = \dot{ts} - \dot{tl}. \tag{14}$$

The signal is passed through gain, a threshold and then integrated.

6) Gravitational ankle torque: The gravitational ankle torque estimator uses ts and $ls = ts - tl$ to calculate the sway angle of the combined COM of the leg and trunk segment. The sway angle of the whole body, bs is determined by

$$bs = \frac{m_l \cdot h_l \cdot ls + m_t(l_l \cdot ls + h_t \cdot ts)}{m_l \cdot h_l + m_t(l_l \cdot h_t)}, \tag{15}$$

when using the small angle approximation. From this, the gravitational torque $T_{g,a}$ is calculated by

$$T_{g,a} = m_b \cdot h_b \cdot bs, \tag{16}$$

where $m_b = m_l + m_t$ and h_b is the height of the combined COM, given by

$$h_b = \frac{m_l \cdot h_l + m_t(l_l + h_t)}{m_b}. \tag{17}$$

The signal $T_{g,a}$ is processed in the same way as $T_{g,h}$.

7) External ankle torque: In the ankle module there are two unknown torques, so the external ankle torque estimator is used to make an estimation of the sum of the two torques. The first is the torque resulting from the external force perturbation applied to the hips, and the second is the internal coupling force that is a result of the movement of the trunk. The net ankle torque is calculated by

$$T_{tot,a} = \ddot{bs} \cdot J_{b,a}, \tag{18}$$

where $\ddot{bs}$ is the bs signal calculated in the gravitational torque estimate, differentiated twice. J_a is the moment of inertia of whole body around the ankle, calculated by

$$J_{b,a} = J_l + m_l \cdot h_l^2 + J_t + m_t(l_l + h_t)^2, \tag{19}$$

when applying the small angle approximation.

8) Foot space tilt: The Foot space tilt estimator is analogous to the leg space estimator

$$\dot{fs} = \dot{ts} - \dot{tl} - l\dot{f}, \tag{20}$$

where the resulting signal $\dot{fs}$ is passed through a filter, a threshold and an integrator.

C. Controller

The disturbance estimations are used to create an error signal for the controllers. The system consists of two control loops: the hip module and the ankle module.

1) Hip module: In the hip module, the trunk is balanced on top of the hip joint. The inertial torque estimate, gravitational hip torque estimate and the external hip torque estimate are summed and converted to a ts representation of the torque, by

$$ts_{T,h} = \frac{T_h}{m_t \cdot g \cdot h_t}. \tag{21}$$

The ts estimate stemming from the sum of the leg space tilt estimate and the tl signal from the hip proprioception are added to form the error signal for the hip controller. The hip controller is a PD controller. A time delay is present to represent the total neural time delay of the hip module. A small passive hip stiffness and damping is added without a time delay to represent the intrinsic and reflexive muscle properties.

2) Ankle module: The ankle module controls the COM of the combined leg and trunk segment. The gravitational ankle torque estimate and the external ankle torque estimate are summed and converted to a bs representation, using

$$bs_{T,a} = \frac{T_a}{m_b \cdot g \cdot h_b}. \tag{22}$$

This is summed with a bs estimate that is converted from the ls estimate, coming from the sum of fs from the foot space tilt estimate and the lf estimate from the ankle proprioception, and the ts estimate coming from the fusion block. The error signal is the sum of $bs_{T,a}$ and the bs estimate. The error signal is fed into the ankle controller, which creates an active ankle torque using a PD controller.

D. Plant

In the plant, the control signals are transformed into a movement. The TMT method [23] was used to determine the equations of motion of the double pendulum, shown in Figure 13. The bodies are described in terms of the generalized coordinates

$$q = \begin{bmatrix} LS \\ TS \end{bmatrix}, \tag{23}$$

where LS and TS are the angles of the legs and trunk segments, respectively, with respect to the vertical.

The coordinates of the two bodies are expressed in terms of the generalized coordinates

$$x_i = T_i(q) = \begin{bmatrix} x_l \\ y_l \\ LS \\ x_t \\ y_t \\ TS \end{bmatrix} = \begin{bmatrix} h_l \sin(LS) \\ h_l \cos(LS) \\ LS \\ l_l \sin(LS) + h_t \sin(TS) \\ l_l \cos(LS) + h_t \cos(TS) \\ TS \end{bmatrix}, \tag{24}$$

where x_l and y_l are the horizontal and vertical movement of the COM of the leg segment, LS is orientation of the legs with respect to the vertical, and x_t, y_t and

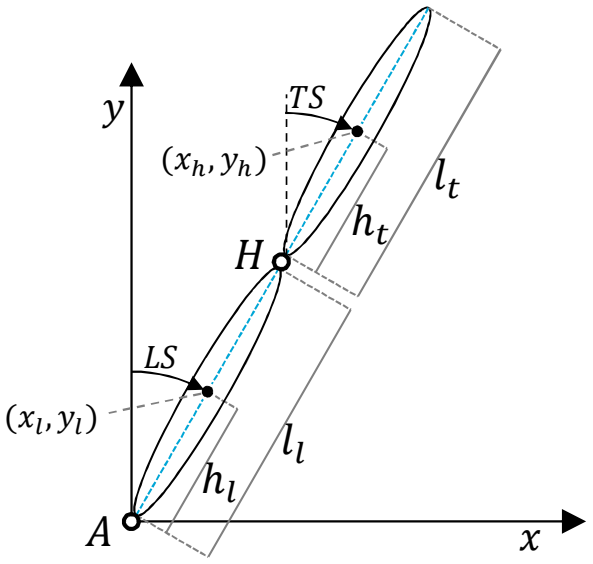

Figure 13: Double pendulum representation of the human body in the sagittal plane, where A is the ankle joint and H is the hip joint.

TS describe the same properties of the trunk segment. Furthermore, h_t is the distance between the ankle joint, A, and the COM of the legs, l_l is the length of the leg segment and h_t is the distance between the hip joint, H, and the COM of the trunk.

The TMT method says that the movement of a multibody system can be described with the formula

$$\overline{M} \cdot \ddot{q} = \overline{f}, \tag{25}$$

where $\overline{M}$ is the reduced mass matrix, $\ddot{q}$ is the second derivative of the generalized coordinates, and $\overline{f}$ is the reduced force vector. The reduced mass matrix and force vector are given by

$$\overline{M} = T^T \cdot M \cdot T \tag{26}$$

$$\overline{f} = T^T \left(\Sigma f - M \cdot g \right), \tag{27}$$

where T is the first order kinematic transfer function, given by

$$T = \frac{\partial T_i}{\partial q}. \tag{28}$$

The force vector, which consists of all the forces and torques applied to the bodies, is given by

$$\Sigma f_i = \begin{bmatrix} F_{x_l} \\ F_{y_l} \\ T_l \\ F_{x_t} \\ F_{y_t} \\ T_t \end{bmatrix} = \begin{bmatrix} F_h \\ -m_l \cdot g \\ T_a - T_h + F_h(l_l - h_l)\cos(LS) \\ F_s \\ m_t \cdot g \\ T_h + F_s(h_s - h_t)\cos(TS) \end{bmatrix}, \tag{29}$$

where F_{x_l}, F_{y_l} and T_l are respectively the horizontal force, vertical force and torque applied to leg segment, and F_{x_t}, F_{y_t} and T_t are the same forces and torques, but acting on the trunk segment. F_h is the external force applied to the hips, F_s is the external force applied to the shoulders, T_a is the sum of active and passive muscle torque around the ankle and T_h is the sum of active and passive muscle torque around the hip joint. The mass matrix M is given by a diagonal matrix with the vector

$$d_m = \begin{bmatrix} m_l & m_l & J_l & m_t & m_t & J_t \end{bmatrix}, \tag{30}$$

on the diagonal, where m_l is the mass of the leg segment, J_l is the moment of inertia of the leg segment around the COM, and m_t and J_t are mass and moment of inertia of the trunk.

The differential equation given in 25 was implemented in Simulink using a Matlab function block, where the input consists of the external forces F_h and F_s, the internally generated torques T_a and T_h and the state variables LS, TS, $\dot{LS}$ and $\dot{TS}$. The output is given by the derivatives of the four state variables, thus $\dot{LS}$, $\dot{TS}$, $\ddot{LS}$ and $\ddot{TS}$, the last two determined by the differential equation 25 and the first two are simply equal to the inputs $\dot{LS}$ and $\dot{TS}$. The four output variables are integrated using integrator blocks.